metals

MDPI

Article

Setting the Basis for the Interpretation of Temperature First Order Reversal Curve (TFORC) Distributions of Magnetocaloric Materials

Luis M. Moreno-Ramírez and Victorino Franco *

Dpto. Física de la Materia Condensada, ICMSE-CSIC, Universidad de Sevilla, P.O. Box 1065, 41080 Sevilla, Spain; lmoreno6@us.es

* Correspondence: vfranco@us.es; Tel.: +34-954-553-886

Received: 10 July 2020; Accepted: 31 July 2020; Published: 2 August 2020

Abstract: First Order Reversal Curve (FORC) distributions of magnetic materials are a well-known tool to extract information about hysteresis sources and magnetic interactions, or to fingerprint them. Recently, a temperature variant of this analysis technique (Temperature-FORC, TFORC) has been used for the analysis of the thermal hysteresis associated with first-order magnetocaloric materials. However, the theory supporting the interpretation of the diagrams is still lacking, limiting TFORC to a fingerprinting technique so far. This work is a first approach to correlate the modeling of first-order phase transitions, using the Bean–Rodbell model combined with a phenomenological transformation mechanism, with the features observed in experimental TFORC distributions of magnetocaloric materials. The different characteristics of the transformations, e.g., transition temperatures, symmetry, temperature range, etc., are correlated to distinct features of the distributions. We show a catalogue of characteristic TFORC distributions for magnetocaloric materials that exhibit some of the features observed experimentally.

Keywords: TFORC; thermal hysteresis; magnetocaloric materials

1. Introduction

Magnetocaloric (MC) materials [1], those that experience a significant temperature change when submitted to magnetic field variations in adiabatic conditions, deserve the attention of the magnetic research community due to their implementation on a new, green and energy efficient solid-state cooling technology at room temperature [2,3]. The effect is associated with significant magnetization changes driven by temperature and magnetic field, classifying the MC materials according to the order of their thermomagnetic phase transition: first- and second-order type [4]. Since the first experiments with pure Gd in 1976 [5], which undergoes a Curie transition (second-order type) from the ferromagnetic (FM) to the paramagnetic (PM) state, the interest has moved nowadays to those magnetocaloric materials which undergo magnetoelastic or magnetostructural transitions (first-order type) such as GdSiGe [6,7], LaFeSi [8,9], MnFePAs [10,11] or Heusler [12,13]-based alloys. Typically, these materials present higher MC response than those with second order transitions, although they have associated undesired thermal and magnetic hysteresis, which significantly reduces its response in cyclical conditions, limiting their applicability in refrigeration devices [14]. Therefore, the understanding of the different sources and mechanisms of hysteresis is a relevant topic in the MC research field [15].

First Order Reversal Curve (FORC) distributions of magnetic materials are a well-recognized tool to extract information about magnetic interactions or to fingerprint magnetic materials [16–18]. Recently, the possibility to use this technique to analyze the thermal hysteresis associated with the first-order magnetocaloric materials has been shown [19,20]. This so called TFORC technique (which is

formally defined analogously to its more conventional field counterpart) is based on the analysis of the minor loops of the magnetization (M) in the hysteretic region, defining a certain set of reversal curves, in an analogous way to what was previously done for spin crossover materials [21]. To measure these curves, first the system is heated up (cooled down) from saturation to a certain temperature (reversal temperature, T_r) and, next, the system is cooled down (heated up) to the initial saturated value while the magnetization values are measured. The set of magnetization curves for different T_r are processed to obtain a TFORC distribution in the case of heating and cooling according to:

$$\rho_C(T, T_r) = -\frac{\partial^2 M_{rev,C}(T, T_r)}{\partial T \partial T_r}, \quad (1)$$

$$\rho_H(T, T_r) = \frac{\partial^2 M_{rev,H}(T, T_r)}{\partial T \partial T_r}, \quad (2)$$

where the subindex C and H refer to the cooling and heating curves, respectively. These distributions are explained in terms of hysteron distributions although a direct connection between the FORC and TFORC distributions and the Preisach model [22] is not usually found. The hysteron is a fundamental hysteresis loop, which is characterized by two switching fields between two stable states called "up" and "down" (the fundamental hysteresis unit) and is defined by two parameters for the thermal hysterons: (1) the hysteron width (T_h) and (2) the central position of the hysteron (T_u). The distributions shown in Equations (1) and (2) can be obtained as a function of these two temperatures by a simple variable change: $T_h = |T - T_r|/2$ and $T_u = (T + T_r)/2$. In the case of conventional FORC, the extensive modelling efforts performed over decades have allowed the extraction of different characteristics of the material from the features found in the distribution [18,23–27]. However, the recent appearance of TFORC in magnetocaloric materials means that there is no fundamental basis that connects TFORC diagrams and the underlying physics of the thermal hysteresis, limiting TFORC to a fingerprinting technique so far.

In this work, we set the basis for the interpretation of TFORC diagrams by performing a systematic study based on modeling of first-order phase transitions using the Bean–Rodbell model [28] extended with a phenomenological transformation mechanism and correlating the obtained diagrams with the characteristics of the transition. The use of skewed normal distributions for modeling the transformation process between FM and PM phases allows the calculation of the reversal magnetization curves, unlike with the pure Bean and Rodbell model. The transformation characteristics explored are: transition temperatures, temperature ranges of the transformations and symmetry/asymmetry of cooling and heating processes. Each of them produce different shapes in the distributions, such as circular, ellipsoidal, semicircular or triangular. This first catalogue of images obtained in this work, analogous to those catalogues available for conventional FORC, can help the interpretation of experimental TFORC distributions.

2. Methods

The Bean–Rodbell model was proposed in 1962, to describe the first-order magnetoelastic transition observed in the MnAs compound [28]. Apart from this material, the model has been successfully applied to other materials that undergo a magnetoelastic first-order transition such as LaFeSi [29,30] and MnFePAs [31,32] alloys, which are of great technological interest. The model assumes that magnetic interactions are affected by such volume changes as:

$$T_t = T_0(1 + \beta\omega), \quad (3)$$

where T_t is the transition temperature, T_0 the transition temperature in absence of deformations (or Curie temperature), β an introduced parameter and ω the relative volume change.

Introducing the assumed dependence shown in Equation (3) into the expression for the Gibbs energy (which considers the Zeeman, exchange, distortion, external pressure and entropy terms in the

framework of mean field theories [28]) and minimizing with respect to ω and M variables, the following expression for M can be obtained:

$$\frac{M}{M_S} = B_J\left(\frac{g\mu_B J}{k_B T}\mu_0 H + \frac{3T_0}{T}\left(\frac{J}{J+1}\right)\frac{M}{M_S} + \eta\frac{9}{10}\left(\frac{2J^2+2J+1}{(J+1)^3}\right)\frac{T_0}{T}\frac{M^3}{{M_S}^3}\right) \quad (4)$$

where M_S is the saturation magnetization, B_J the Brillouin function, g the Landé factor, μ_B the Bohr magneton, J the total quantum angular momentum, μ_0 the vacuum permeability, H the magnetic field and η a parameter of the model, defined as:

$$\eta = \frac{5}{2}\left(\frac{(2J+1)^4-1}{(2(J+1))^4}\right)\frac{M_S}{g\mu_B J}k_B T_0 k\beta^2, \quad (5)$$

where k is the compressibility. The η parameter controls the order of the transition, being first-order if $\eta > 1$, second-order if $\eta < 1$ and $\eta = 1$ corresponds to the critical point (where the order of the transition changes from second to first). T has a single-valued solution as a function of M and H in Equation (4). For $\eta > 1$, metastable and instable regions appear in the solution. The stable solution is obtained when the energy of FM and PM phases are the same (being $T_{t,ST}$, the transition temperature of the stable branch), which is calculated according to the so-called equal-area construction from the single-valued solution. The existence of the metastable branches leads to two different solutions when the material is under heating or cooling conditions ($T^H_{t,MS}$ and $T^C_{t,MS}$), which gives rise to associated hysteresis. For simulating the Bean–Rodbell model, the following parameters have been used in this work: $g = 2$, $J = 7/2$, $M_S = 1.96 \times 10^6$ A·m^{-1}, $T_0 = 300$ K, $k = 2.5{\cdot}\times 10^{-11}$ Pa^{-1} and $\beta = 13.54$ ($\eta = 1.5$). These parameters are arbitrarily chosen to represent a first-order phase transition material with a transition temperature close to room temperature. Figure 1 shows the temperature dependence of the Bean–Rodbell solution for a magnetic field of 0.01 T.

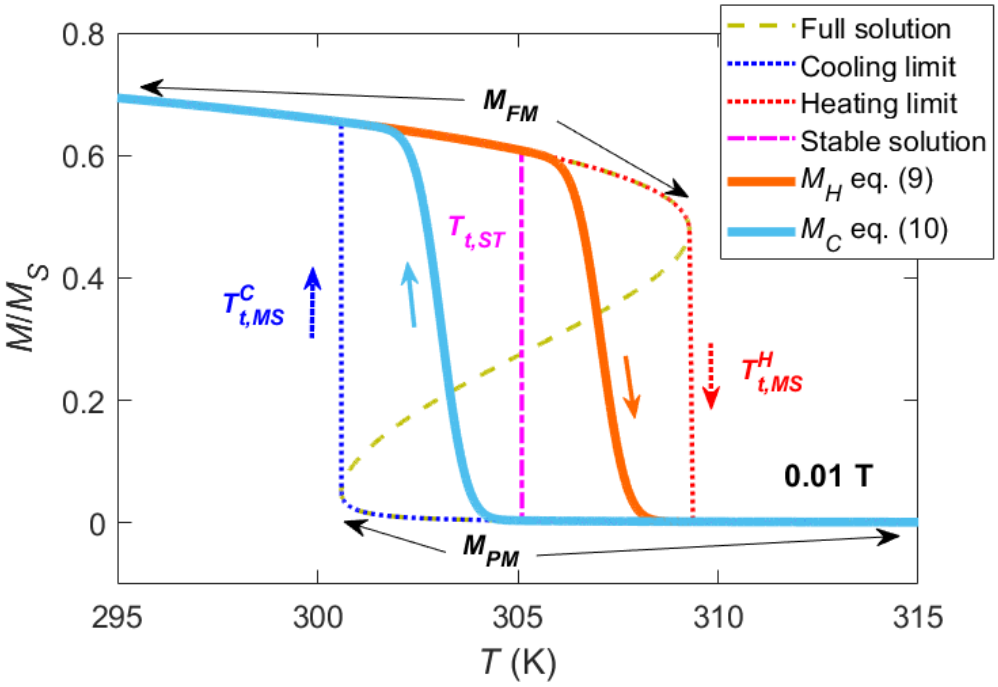

Figure 1. Temperature dependence of M from the pure Bean–Rodbell model (discontinuous lines) and the proposed modeling introducing a transformation process with specified parameters, $T^H_{t,MS}$ = 307 K, $T^C_{t,MS}$ = 305 K and $\sigma_H = \sigma_C = 0.5$ K, into the Bean–Rodbell model (continuous lines).

In the framework of the pure Bean–Rodbell model, the transformation between both FM and PM phases is described as just an abrupt step in temperature (or magnetic field) between the values corresponding to both phases. This feature does not agree with the observations of first-order transitions in which coexistence between phases is intrinsic to the nature of the phase transition (and crucial for understanding FORC distributions). To reproduce the transformed fraction (f) through the first-order transition, we propose the modeling through the cumulative distribution function of a skewed normal distribution [33] as:

$$f(T) = \frac{1}{2}\left[1 + \mathrm{erf}\left(\frac{T-\xi}{\sqrt{2}\sigma}\right)\right] - 2\,O_T\left(\frac{T-\xi}{\sigma}, \alpha\right), \quad (6)$$

where erf is the error function and O_T is the Owen's T function. The different parameters are ξ which is the location, σ the scale and α the shape or skewness factor (which can be either positive or negative). For this distribution, the mean value is $\xi + \sigma\frac{\alpha}{\sqrt{1+\alpha^2}}\sqrt{\frac{2}{\pi}}$ and the variance is $\sigma^2(1-\frac{2\alpha^2}{\pi(1+\alpha^2)})$. It is observed that for $\alpha = 0$, the normal distribution function is recovered (as $\mathrm{O_T}(\alpha = 0) = 0$). This phenomenological skewed normal distribution function can be linked to different transformation characteristics of the materials, such as nucleation-growth processes, transition temperature distributions (caused by compositional inhomogeneities) or internal stress effects, among others. Some of these details of the transformation can be directly identified (as will be mentioned later); for others (e.g., to distinguish between compositional inhomogeneities or kinetic processes), a detailed analysis of the samples using complementary techniques would be required. To be able to obtain a hysteretic behavior, the parameters of the transformed function (i.e., ξ, σ and α) while heating (FM to PM transformation) or cooling (PM to FM transformation) should be different. Therefore, two transformed functions, f_H and f_C, are defined for the heating and cooling processes, respectively:

$$f_H(T) = \frac{1}{2}\left[1 + \mathrm{erf}\left(\frac{T-\xi_H}{\sqrt{2}\sigma_H}\right)\right] - 2\,\mathrm{O_T}\left(\frac{T-\xi_H}{\sigma_H}, \alpha_H\right), \quad (7)$$

$$f_C(T) = \frac{1}{2}\left[1 + \mathrm{erf}\left(\frac{\xi_C-T}{\sqrt{2}\sigma_C}\right)\right] - 2\,\mathrm{O_T}\left(\frac{\xi_C-T}{\sigma_C}, \alpha_C\right). \quad (8)$$

Then by knowing the magnetization curves of both FM and PM phases, M_{FM} and M_{PM}, respectively, which are obtained from the Bean–Rodbell model (shown in Figure 1), the magnetization for the heating and cooling processes are expressed as:

$$M_H = (1-f_\mathrm{H})M_\mathrm{FM} + f_\mathrm{H}M_\mathrm{PM}, \quad (9)$$

$$M_C = f_\mathrm{C}M_\mathrm{FM} + (1-f_\mathrm{C})M_\mathrm{PM}. \quad (10)$$

According to the Bean–Rodbell model, we assume a transformation process only in the metastable temperature region. Therefore, the transformed function for any set of parameters should fulfil that $f_\mathrm{H}(T_{t,ST}) = f_\mathrm{C}(T_{t,ST}) = 0$ and $f_\mathrm{H}(T^H_{t,MS}) = f_\mathrm{C}(T^\mathrm{C}_{t,MS}) = 1$ (i.e., the transformation cannot be extended further than the metastable region). An example of the modeled magnetization curves that can be obtained is included in Figure 1 using the normal distribution with $T^H_{t,MS}$ = 307 K, $T^C_{t,MS}$ = 305 K and $\sigma_H = \sigma_C = 0.5$ K. This kind of approximation in which the Bean–Rodbell model is combined with a transformation process has been applied successfully to the description of the hysteresis in MC materials [34].

Once the transformed fractions together with the magnetization values are obtained for both heating and cooling processes, the different reversal magnetization curves can be derived as a function of the temperature and the reversal temperature (according to the measurement protocol explained in the introduction) as:

$$M_{\mathrm{rev,C}}(T,T_r) = (1-f_H(T_r))M_\mathrm{FM}(T) + f_H(T_r)[f_\mathrm{C}(T)M_\mathrm{FM}(T) + (1-f_\mathrm{C}(T))M_\mathrm{PM}(T)], \quad (11)$$

$$M_{\mathrm{rev,H}}(T,T_r) = (1-f_C(T_r))M_{\mathrm{PM}}(T) + f_C(T_r)[(1-f_{\mathrm{H}}(T))M_{\mathrm{FM}}(T) + f_{\mathrm{H}}(T)M_{\mathrm{PM}}(T)]. \quad (12)$$

As an example, minor hysteresis loops to obtain the first order reversal magnetization curves while cooling and heating are shown in Figure 2. With these reversal curves, the TFORC distributions are calculated using Equations (1) and (2).

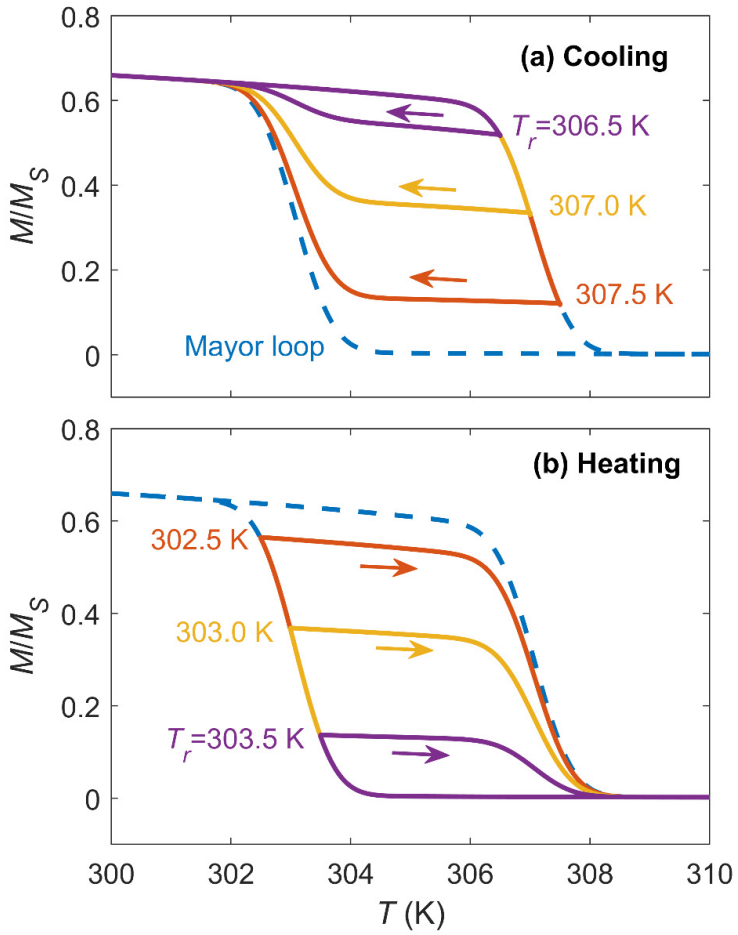

Figure 2. First order reversal magnetization curves for cooling (**a**) and heating (**b**) processes (Equations (11) and (12), respectively) from the major hysteresis loop from Figure 1.

3. Results and Discussion

3.1. Symmetric Transformations

First, we tested the simplest cases for which both heating and cooling process are symmetric ($\alpha_H = \alpha_C = 0$, the resulting distribution being the usual normal distribution) and both have the same transition temperature range ($\sigma_H = \sigma_C$), i.e., the FM to PM transformation is equivalent to the PM to FM one. The only difference is the location parameter of both processes (ξ_H and ξ_C). This symmetric transformation is typically ascribed to nucleation-growth phenomena or to transition temperature distributions.

Figure 3a′–d′ shows the obtained cooling TFORC diagrams (which are accompanied by their corresponding first order reversal magnetization curves Figure 3a–d) under different conditions (different transition temperatures and different ranges of the transformation). As a general feature, we observe a circular TFORC distribution around a maximum at certain coordinates (T_u, T_h). In addition to that, and only for temperatures far from the maximum of the distribution, deviations from the circular shape can be observed (further discussed below). We can observe that the maximum distribution values are only dependent on the values of the transition temperatures while the radius distributions

depend only on the σ values, increasing as the σ values increase. For the normal distribution, just the σ parameter is related to the transformation range (e.g., as the variance is only dependent on σ). The coordinates of the maxima coincide with the center of the loop (T_{center}) in the T_h axis and with the half width of the hysteresis loop (ΔT_{loop}) in the T_h axis. On the one hand, T_{center} can be experimentally calculated as the average value of the temperatures that make maximum $\partial M/\partial T$ for both heating and cooling processes. On the other hand, ΔT_{loop} can be calculated as the half of the difference between the temperatures that make maximum $\partial M/\partial T$ for both heating and cooling processes. The maximum value of the distribution is highly dependent on the transformation range, increasing as the transformation range decreases.

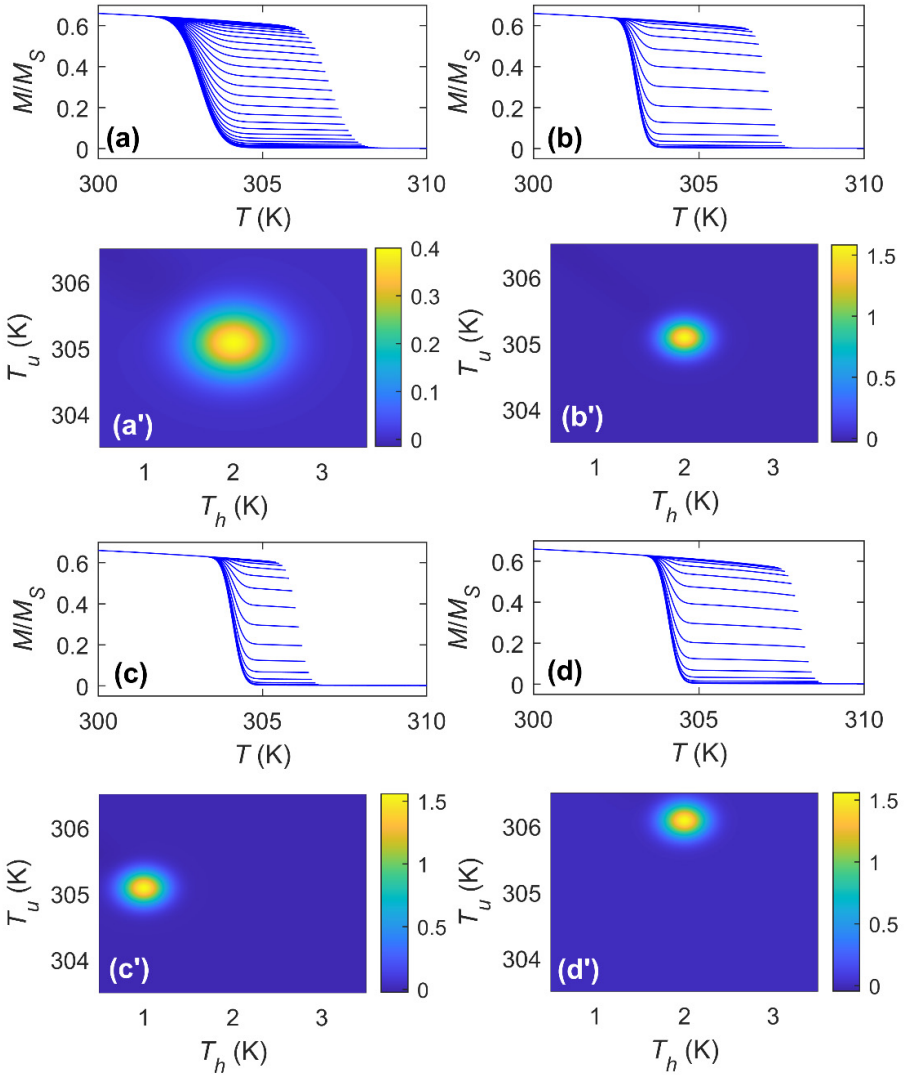

Figure 3. Cooling first order reversal magnetization curves and associated Temperature First Order Reversal Curve (TFORC) distributions with different transformation characteristics: (**a**–**a'**) $\xi_H = T_{t,ST} + 2$ K, $\xi_C = T_{t,ST} - 2$ K and $\sigma_H = \sigma_C = 0.5$ K, (**b**–**b'**) $\xi_H = T_{t,ST} + 2$ K, $\xi_C = T_{t,ST} - 2$ K and $\sigma_H = \sigma_C = 0.25$ K, (**c**–**c'**) $\xi_H = T_{t,ST} + 1$ K, $\xi_C = T_{t,ST} - 1$ K and $\sigma_H = \sigma_C = 0.25$ K and (**d**–**d'**) $\xi_H = T_{t,ST} + 3$ K, $\xi_C = T_{t,ST} - 1$ K and $\sigma_H = \sigma_C = 0.25$ K. (For all the cases, the skewness factors are zero).

However, as mentioned above, for low ρ_C. values (far from the maximum), a tail of small negative values located along the 135° line with respect the maximum can be observed for all the diagrams. When analyzing the heating TFORC in comparison to the cooling one (shown in Figure 4 a',b'), only positive values are obtained and now a small tail with positive values is located along the 225° line

with respect to the maximum (this difference will be justified below). Apart from these features at low ρ values, both cooling and heating TFORC distributions are equivalent (it has also been proven for all the other cases studied in this work, even if not explicitly mentioned again). Slightly higher values of ρ. are obtained for the cooling compared to the heating one, being ascribed to the larger magnetization jump at the transition for the cooling curve. The origin of the observed tails is related to the different temperature evolution of the FM and PM phases, and the transformation processes have no influence on it, as can be mathematically demonstrated for the cooling case (heating would be analogous). Starting from Equation (11), $\rho_C(T, T_r)$ can be analytically calculated from Equation (1) leading to:

$$\rho_C(T, T_r) = \frac{\partial f_H}{\partial T_r}\left((1 - f_C)\frac{\partial \Delta M}{\partial T} - \frac{\partial f_C}{\partial T}\Delta M\right) \quad (13)$$

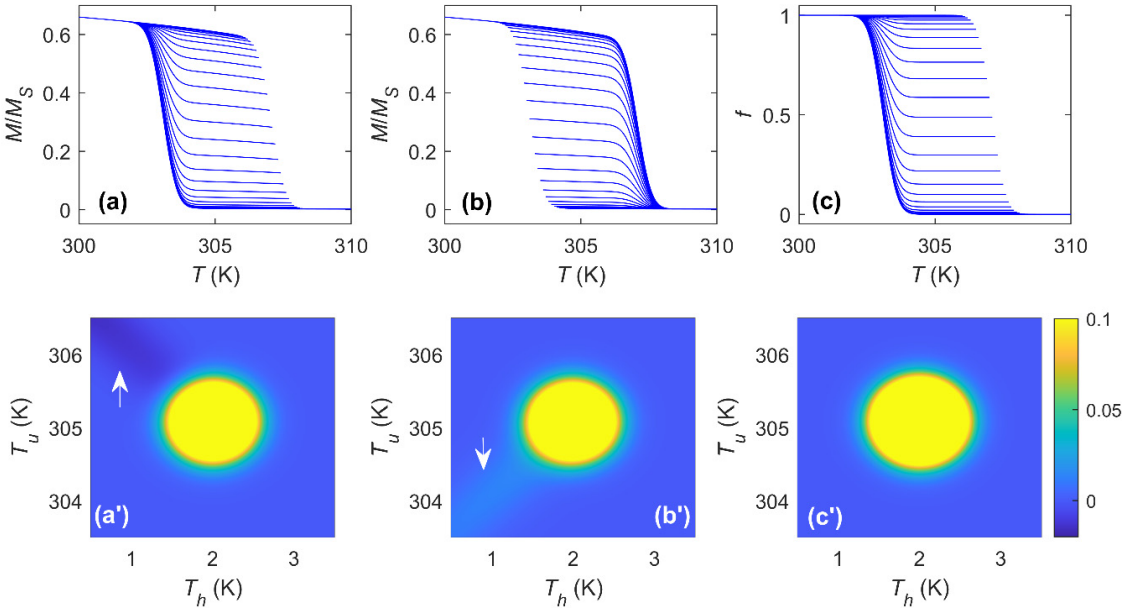

Figure 4. First order reversal magnetization curves and associated TFORC distributions with $\xi_H = T_{t,ST} + 2$ K, $\xi_C = T_{t,ST} - 2$ K, $\sigma_H = \sigma_C = 0.4$ K (skewness not considered) for (**a**–**a'**) cooling and (**b**–**b'**) heating. (**c**–**c'**) Cooling reversible magnetization curves and TFORC distributions using only the transformed phase fraction.

As $\Delta M = M_{FM} - M_{PM}$. As $\partial f_H / \partial T_r$ is always positive, the sign of the distribution is given by the sign of the bracket. On the one hand, we can see that the second term inside the bracket $(-\frac{\partial f_C}{\partial T}\Delta M)$ is always positive (its minimum value is 0) as $\partial f_C / \partial T$ is negative and ΔM positive. On the other hand, the sign of the first term depends on the sign of $\partial \Delta M / \partial T$, as $(1 - f_C)$ is always positive. Close to the heating branch of the hysteresis loop, this term is negative (as can be easily inferred from Figure 1) while $\partial f_C / \partial T \cong 0$ and then, the distribution takes negative values. This fits with the observations, as negative values are obtained for $T_u > T_{center}$ and $T_h < \Delta T_{loop}$. The same analysis can be done for the heating distribution (from Equations (2) and (12)), the result being in agreement with the observation of Figure 4b'. As we conclude that the observed tails come from the temperature dependence on FM and PM magnetization, it is possible to check this feature if we just reduce M_{FM} and M_{PM} to 1 and 0, respectively. Making this, the resulting TFORC is just dependent on the transformation characteristics. Figure 4c' shows the cooling TFORC distribution without magnetization contribution for the cooling process, and it is clearly observed that previous tails do not appear (in agreement with the previous arguments). In fact, despite those tails, both distributions are quite similar to the ones using magnetization data, illustrating that TFORC is a useful tool to extract information on the transformation processes. At this point, it has to be mentioned that the general features of the

transformation (e.g., asymmetry or width) could also be extracted from magnetization curves. However, $M(T)$ curves along the transformation are considerably affected by the temperature dependence of the magnetic moment of the pure phases (mainly the FM) jeopardizing the extraction of transformed functions from magnetization data. Moreover, TFORC would make it possible to discern the case of several transformation processes during the transformation (possibly emerging from coexisting phases), which would not be evident from the simple observation of the $M(T)$ curves, analogously to the advantages of conventional FORC vs. $M(H)$ curves. These various transformation processes have been evidenced by TFORC in [19].

Next, we checked the cases for which both heating and cooling processes remain symmetric ($\alpha_H = \alpha_C = 0$) but with different transition ranges ($\sigma_H \neq \sigma_C$). Figure 5a′–c′ shows the cooling TFORC distribution for different σ (for simplification, the transition temperatures are $\xi_H = T_{t,ST} + 2$ K and $\xi_C = T_{t,ST} - 2$ K for all the cases). It can be observed that as the difference between σ_H and σ_C appears, the circular behavior (shown in Figure 3a′) changes to a rotated ellipse for which its major symmetry axis is located along the +45° line with respect the maximum if $\sigma_H > \sigma_C$. As the difference between σ_H and σ_C increases, the ellipse becomes narrower. When $\sigma_C > \sigma_H$, the major symmetry axis of the ellipse is rotated 90°. This observation highlights that not only the shape of the distribution is important but the orientation also gives us useful information. It can be noted that, although the shape is not circular, the ellipse keeps its center at $T_u = T_{center}$ and $T_H = \Delta T_{loop}$.

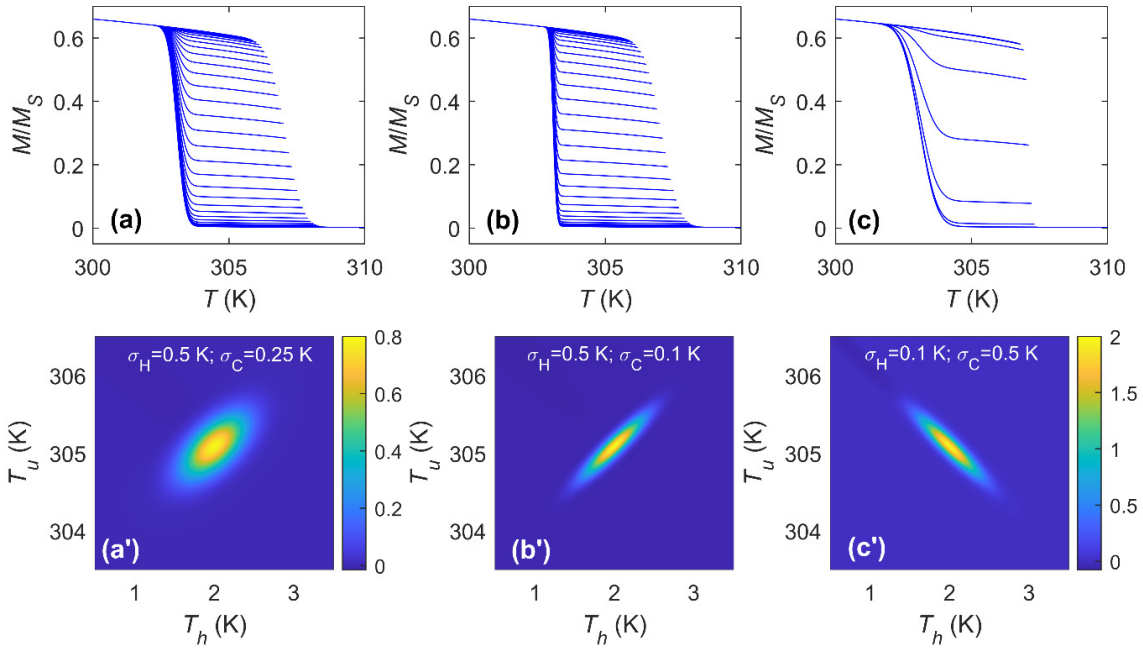

Figure 5. Cooling first order reversal magnetization curves and associated TFORC distributions with $\xi_H = T_{t,ST} + 2$ K, $\xi_C = T_{t,ST} - 2$ K (skewness not considered) for (**a**–**a′**) $\sigma_H = 0.5$ K and $\sigma_C = 0.25$ K, (**b**–**b′**) $\sigma_H = 0.5$ K and $\sigma_C = 0.1$ K and (**c**–**c′**) $\sigma_H = 0.1$ K and $\sigma_C = 0.5$ K.

3.2. Asymmetric Transformations

We can introduce asymmetry in the transformation processes by using non-null α_H and α_C factors in the model. This asymmetry of the transformations has been observed in experimental data and is typically linked to internal stress/constrains during the transformations [35,36]. At the first stages of the transformation, the emerging nuclei can grow without interaction (contact) with others, but growth is hindered at final stages (reducing the rate) by the effect of the nearby transformed fractions (potentially leading to the existence of kinetic arrest). With the proposed model, we are able to reproduce: (1) transitions for which the transformation rate is faster at initial stages and (2) transformations with slower rates at initial stages. These two features can be reproduced using

positive and negative α parameters, respectively. To illustrate them, the temperature dependence of the magnetization at the transition and its derivative with respect the temperature using different α parameters are shown in Figure 6. When the skewness is not considered (as was the case up to this section), the curves are symmetric (i.e., the maximum transformation rate occurs at the middle of the transformation), as can be observed in the derivative. When skewness is introduced, the distribution becomes asymmetric, with the maximum being shifted either to low transformed fractions when α is positive (i.e., the process is faster at the beginning of the transformation, before $f = 0.5$) or to high transformed fractions when α is negative (i.e., the process is faster at the end of the transformation, after $f = 0.5$). In this simple way, the possible transformation cases can be qualitatively modeled without the necessity of introducing complicated kinetic theories.

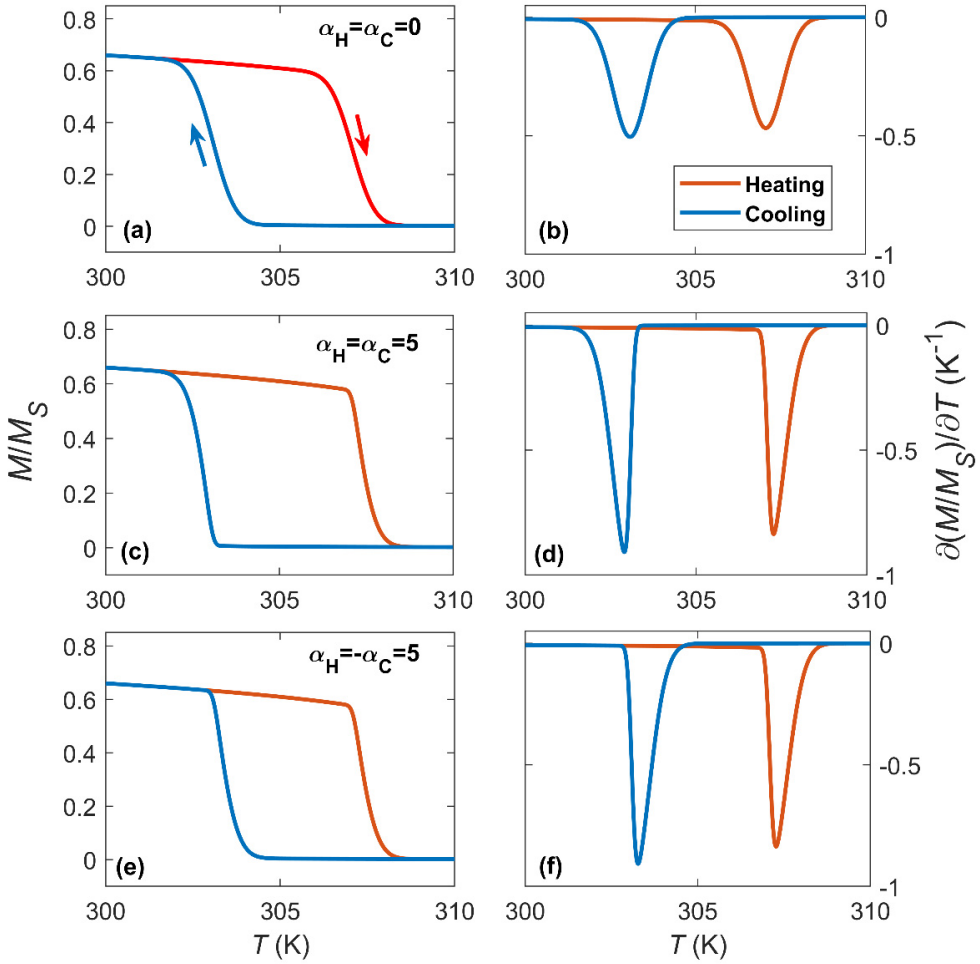

Figure 6. Temperature dependence of the magnetization and its first derivative with respect to the temperature with $\xi_H = T_{t,ST} + 2$ K, $\xi_C = T_{t,ST} - 2$ K, $\sigma_H = \sigma_C = 0.5$ K and (**a**,**b**) $\alpha_H = \alpha_C = 0$, (**c**,**d**) $\alpha_H = \alpha_C = 5$, (**e**,**f**) $\alpha_H = -\alpha_C = 5$.

Figure 7 a'–d' shows the TFORC distributions when considering that one process is asymmetric while the other remains symmetric, using different combination of the skewness factors (keeping the other parameters fixed to $\xi_H = T_{t,ST} + 2$ K, $\xi_C = T_{t,ST} - 2$ K, $\sigma_H = \sigma_C = 0.5$ K). It can be observed that the TFORC distribution has a semicircular-like shape. The semicircular shape is more evident as the asymmetry factor increases (Figure 7a',b'). Moreover, the orientation of the semicircle depends on the different combinations of parameters. The orientation is denoted with respect to the symmetry axis (which is the reflection axis). When the asymmetric transformation is the cooling one, the semicircle is orientated along 135° or 315° for positive and negative α values, respectively (Figure 7c',d'). Similarly, when the asymmetric transformation is the heating one, the semicircle is orientated along 45° or 225°

for positive and negative α values, respectively. It should be noted that when introducing non-negative α values, the temperature range is no longer dependent only on σ (although it is the main factor) and therefore, the heating and cooling processes have slightly different transformation ranges.

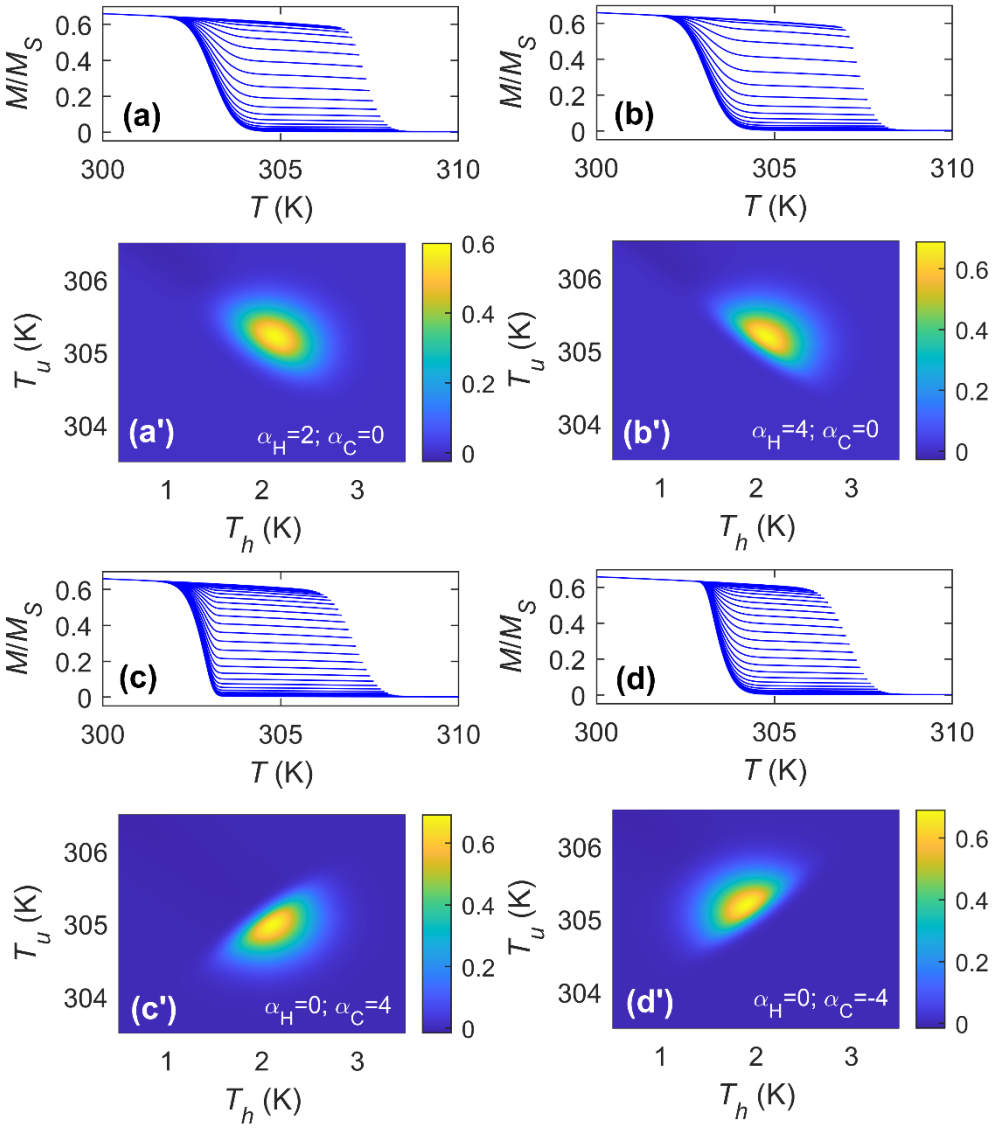

Figure 7. Cooling first order reversal magnetization curves and associated TFORC distributions with $\xi_H = T_{t,ST} + 2$ K, $\xi_C = T_{t,ST} - 2$ K, $\sigma_H = \sigma_C = 0.5$ K and different skewness factor combinations: (**a**–**a′**) $\alpha_H = 2$, $\alpha_C = 0$, (**b**–**b′**) $\alpha_H = 4$, $\alpha_C = 0$, (**c**–**c′**) $\alpha_H = 0$, $\alpha_C = 4$ and (**d**–**d′**) $\alpha_H = 0$, $\alpha_C = -4$.

Different situations when both transformation processes are considered asymmetric (same α factors) are illustrated in Figure 8a′–d′, for which $\xi_H = T_{t,ST} + 2$ K, $\xi_C = T_{t,ST} - 2$ K, $\sigma_H = \sigma_C = 0.5$ K have been kept constant. It is inferred from the plots that TFORC distributions have isosceles triangle-like shape. It should be noted that as σ and α heating and cooling factors have the same absolute value, the transformation range is the same. It is observed that one vertex of the triangle is always pointing to the central coordinate (i.e., $T_u = T_{center}$ and $T_h = \Delta T_{loop}$) but its reflection symmetry axis is oriented with different angles, 0, 90, 180 and 270° for $\alpha_H = \alpha_C > 0$, $\alpha_H = -\alpha_C > 0$, $\alpha_H = -\alpha_C < 0$ and $\alpha_H = \alpha_C < 0$, respectively. It is worth noting that the orientations observed for the triangular distributions are not the same of those semicircular ones. If both skewness factors are different, the isosceles triangle is modified to a scalene one as the triangle does not have any symmetry axis.

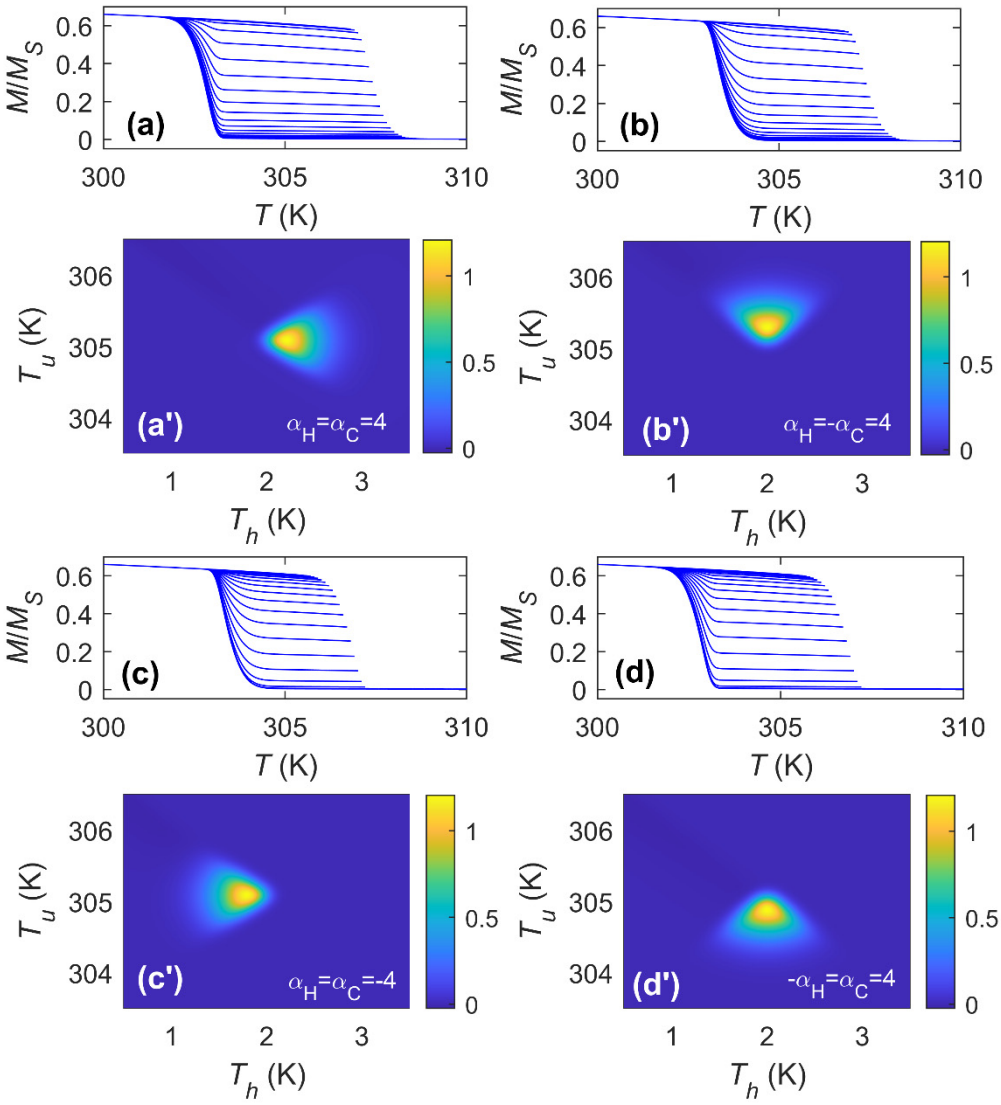

Figure 8. Cooling first order reversal magnetization curves and associated TFORC distributions with $\xi_H = T_{t,ST} + 2$ K, $\xi_H = T_{t,ST} - 2$ K, $\sigma_H = \sigma_C = 0.5$ K and different skewness factor combinations: (**a**–**a′**) $\alpha_H = \alpha_C = 4$, (**b**–**b′**) $\alpha_H = -\alpha_C = 4$, (**c**–**c′**) $\alpha_H = \alpha_C = -4$ and (**d**–**d′**) $-\alpha_H = \alpha_C = 4$.

Another possible effect in addition to both asymmetric processes is that both transformations also present different σ parameters (as mentioned before, with σ being the main factor affecting the transformation range). We take as an example the previous case with $\alpha_H = \alpha_C = 4$ (shown in Figure 8a′) with different σ values when cooling and heating, illustrated in Figure 9a′–c′. When $\sigma_H = \sigma_C$ the distribution has a triangular-like shape, as previously observed. However, when $\sigma_H \neq \sigma_C$ the triangle shape is distorted. The distortion produced is quite similar to the one studied previously in Figure 5. It can be observed that as the difference between σ_H and σ_C increases, the triangular-like shape is distorted, becoming elongated along the 45° line if $\sigma_H > \sigma_C$ (Figure 9a′). If $\sigma_H < \sigma_C$, the elongation is produced along the −45° line, this being more significant as the differences increase (Figure 9b′,c′). The isosceles triangle is modified to a scalene one (similar to the case when α are different) if the differences between σ_H and σ_C are not significant, or to a skewed ellipse if the differences are quite relevant.

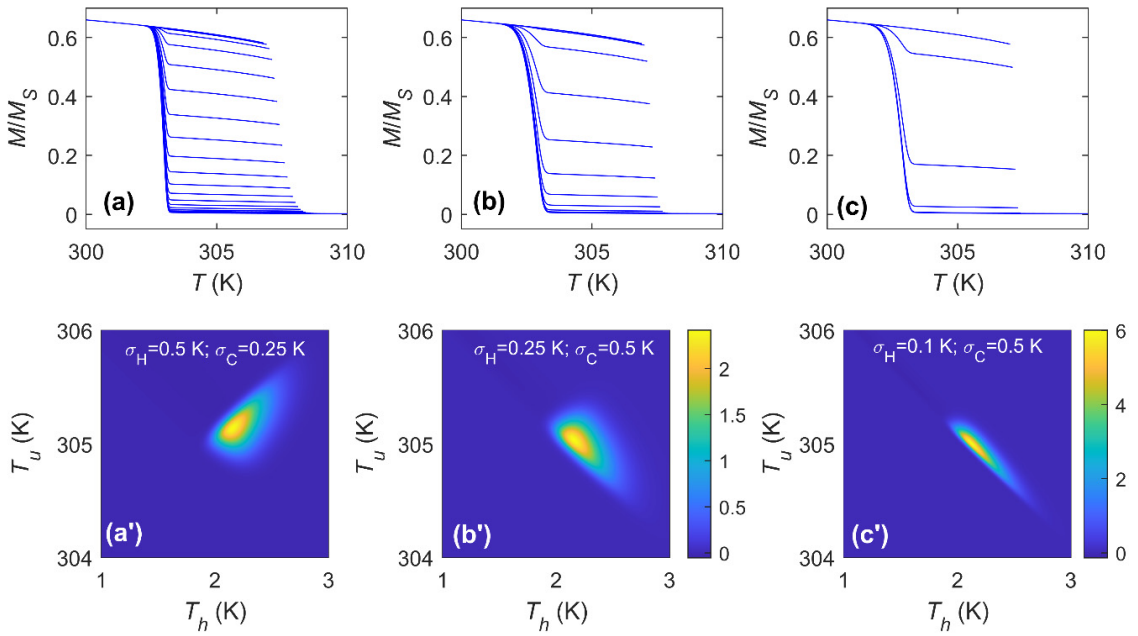

Figure 9. Cooling first order reversal magnetization curves and associated TFORC distributions with $\xi_H = T_{t,ST} + 2$ K, $\xi_C = T_{t,ST} - 2$ K, $\alpha_H = \alpha_C = 4$ and (**a**–**a′**) $\sigma_H = 0.5$ K, $\sigma_C = 0.25$ K, (**b**–**b′**) $\sigma_H = 0.25$ K, $\sigma_C = 0.5$ K, (**c**–**c′**) $\sigma_H = 0.1$ K, $\sigma_C = 0.5$ K.

In order to summarize the main results of the work, the different characteristic TFORC distributions as a function of the transformation parameters (σ and α) are tabulated in Table 1. It is worth mentioning that the published TFORC distributions of magnetocaloric materials [19] include some of the features predicted in this work, like triangular shaped maxima and multiple peaks corresponding to multiple transitions. The combination of the FORC distribution catalogue with the details of the transformation function will make it possible to interpret the features giving rise to the hysteresis in magnetocaloric materials and eventually lead to designing strategies to minimize the irreversibility of the transformation. At the same time, the knowledge of the minor loops allows the implementation of more accurate models for the simulation of the performance of magnetocaloric devices.

Table 1. Summary of some characteristic TFORC distributions according to the transformation features.

Heating Transformation	Cooling Transformation	TFORC Distribution Shape	TFORC Distribution Orientation
$\sigma_H \neq 0$ $\alpha_H = 0$	$\sigma_C = \sigma_H$ $\alpha_C = 0$	Circle	-
$\sigma_H \neq 0$ $\alpha_H = 0$	$\sigma_C < \sigma_H$ $\alpha_C = 0$	Ellipse	45° (major symmetry axis)
$\sigma_H \neq 0$ $\alpha_H = 0$	$\sigma_C > \sigma_H$ $\alpha_C = 0$	Ellipse	−45° (major symmetry axis)
$\sigma_H \neq 0$ $\alpha_H > 0$	$\sigma_C = \sigma_H$ $\alpha_C = 0$	Semi-circle	45° (reflection axis)
$\sigma_H \neq 0$ $\alpha_H = 0$	$\sigma_C = \sigma_H$ $\alpha_C < 0$	Semi-circle	135° (reflection axis)
$\sigma_H \neq 0$ $\alpha_H < 0$	$\sigma_C = \sigma_H$ $\alpha_C = 0$	Semi-circle	225° (reflection axis)
$\sigma_H \neq 0$ $\alpha_H = 0$	$\sigma_C = \sigma_H$ $\alpha_C > 0$	Semi-circle	315° (reflection axis)

Table 1. *Cont.*

Heating Transformation	Cooling Transformation	TFORC Distribution Shape	TFORC Distribution Orientation
$\sigma_H \neq 0$ $\alpha_H > 0$	$\sigma_C = \sigma_H$ $\alpha_C > 0$	Isosceles Triangle	0° (reflection axis)
$\sigma_H \neq 0$ $\alpha_H > 0$	$\sigma_C = \sigma_H$ $\alpha_C < 0$	Isosceles Triangle	90° (reflection axis)
$\sigma_H \neq 0$ $\alpha_H < 0$	$\sigma_C = \sigma_H$ $\alpha_C < 0$	Isosceles Triangle	180° (reflection axis)
$\sigma_H \neq 0$ $\alpha_H < 0$	$\sigma_C = \sigma_H$ $\alpha_C > 0$	Isosceles Triangle	270° (reflection axis)
$\sigma_H \neq 0$ $\alpha_H \neq 0$	$\sigma_C \neq \sigma_H$ $\alpha_C \neq 0$	Combination of previous shapes: scalene triangle or skew ellipse	-

4. Conclusions

Through the modeling of first-order thermomagnetic transitions using the Bean–Rodbell model extended with phase transformation processes by skew normal distributions, it has been possible to extract information of TFORC distributions for magnetocaloric materials. It is relevant to highlight that a TFORC distribution (measured either upon cooling or upon heating) contains information of both cooling and heating transformations. In the simplest case, for which both heating and cooling transitions are symmetric and equivalent, the TFORC distribution has a circular shape around a maximum value. When both transitions are symmetric but with different temperature ranges, the TFORC distribution has an ellipsoidal shape with the major symmetry axis along the 45° (if the heating process is broader than the cooling one) or −45° lines (if the cooling process is broader than the heating one). If one transformation is asymmetric, the TFORC distribution has a semicircular-like shape, the reflection axis oriented along 45, 135, 225 and 315° if $\alpha_H > 0$ and $\alpha_C = 0$, $\alpha_H = 0$ and $\alpha_C < 0$, $\alpha_H < 0$ and $\alpha_C = 0$ and $\alpha_H = 0$ and $\alpha_C > 0$, respectively. When it is considered that both transformations are asymmetric (the maximum transformation rate occurs before or after the center of the transformation temperature span), the TFORC distribution has an isosceles triangular-like shape with its reflection axis along 0, 90, 180 and 270° orientations for $\alpha_H = \alpha_C > 0$, $\alpha_H = -\alpha_C > 0$, $\alpha_H = -\alpha_C < 0$ and $\alpha_H = \alpha_C < 0$, respectively. Finally, it is observed that when the transformations are asymmetric and occur with different transformation ranges, the triangular-like shape becomes distorted along the 45° (if the heating process is broader than the cooling one) or 315° lines (if the cooling process is broader than the heating one), obtaining scalene triangle or skewed ellipse shapes. This information can be useful when analyzing TFORC distributions of first-order MC materials and sets the basis for correlating the observed TFORC distributions with characteristics of the transformation.

Author Contributions: Conceptualization of the work by V.F. and L.M.M.-R.; resources by V.F.; software by L.M.M.-R.; data analysis and validation by L.M.M.-R. and V.F.; original draft preparation by L.M.M.-R.; review and editing by V.F. and L.M.M.-R. All authors have read and agreed to the published version of the manuscript.

Funding: Work supported by AEI/FEDER-UE (grants MAT-2016-77265-R and PID2019-105720RB-I00), US/JUNTA/FEDER-UE (grant US-1260179); Consejería de Economía, Conocimiento, Empresas y Universidad de la Junta de Andalucía (grant P18-RT-746); Army Research Laboratory under Cooperative Agreement Number W911NF-19-2-0212 and Sevilla University under the VI PPIT-US program. Luis M. Moreno-Ramírez acknowledges a postdoctoral fellowship from Sevilla University under the VI PPIT-US program.

Conflicts of Interest: The authors declare no conflict of interest.

References

1. Franco, V.; Blázquez, J.S.; Ipus, J.J.; Law, J.Y.; Moreno-Ramírez, L.M.; Conde, A. Magnetocaloric effect: From materials research to refrigeration devices. *Prog. Mater. Sci.* **2018**, *93*, 112–232. [CrossRef]
2. Yu, B.; Liu, M.; Egolf, P.W.; Kitanovski, A. A review of magnetic refrigerator and heat pump prototypes built before the year 2010. *Int. J. Refrig.* **2010**, *33*, 1029–1060. [CrossRef]
3. Kitanovski, A.; Tušek, J.; Tomc, U.; Plaznik, U.; Ozbolt, M.; Poredoš, A. *Magnetocaloric Energy Conversion*; Springer International Publishing: Cham, Switzerland, 2016; ISBN 978-3-319-08741-2.
4. Jaeger, G. The Ehrenfest Classification of Phase Transitions: Introduction and Evolution. *Arch. Hist. Exact Sci.* **1998**, *53*, 51–81. [CrossRef]
5. Brown, G. V Magnetic heat pumping near room temperature. *J. Appl. Phys.* **1976**, *47*, 3673–3680. [CrossRef]
6. Pecharsky, V.K.; Gschneidner, K.A., Jr. Giant Magnetocaloric Effect in $Gd_5(Si_2Ge_2)$. *Phys. Rev. Lett.* **1997**, *78*, 4494–4497. [CrossRef]
7. Biswas, A.; Mudryk, Y.; Pathak, A.K.; Zhou, L.; Pecharsky, V.K. Managing hysteresis of $Gd_5Si_2Ge_2$ by magnetic field cycling. *J. Appl. Phys.* **2019**, *126*, 243902. [CrossRef]
8. Fujita, A.; Fujieda, S.; Hasegawa, Y.; Fukamichi, K. Itinerant-electron metamagnetic transition and large magnetocaloric effects in $La(Fe_x,Si_{1-x})_{13}$ compounds and their hydrides. *Phys. Rev. B* **2003**, *67*, 104416. [CrossRef]
9. Moreno-Ramírez, L.M.; Romero-Muñiz, C.; Law, J.Y.; Franco, V.; Conde, A.; Radulov, I.A.; Maccari, F.; Skokov, K.P.; Gutfleisch, O. Tunable first order transition in $La(Fe,Cr,Si)_{13}$ compounds: Retaining magnetocaloric response despite a magnetic moment reduction. *Acta Mater.* **2019**, *175*, 406–414. [CrossRef]
10. Tegus, O.; Brück, E.; Buschow, K.H.J.; de Boer, F.R. Transition-metal-based magnetic refrigerants for room-temperature applications. *Nature* **2002**, *415*, 150–152. [CrossRef]
11. Hu, S.; Miao, X.; Liu, J.; Ou, Z.; Cong, M.; Haschuluu, O.; Gong, Y.; Qian, F.; You, Y.; Zhang, Y.; et al. Small hysteresis and giant magnetocaloric effect in Nb-substituted $(Mn,Fe)_2(P, Si)$ alloys. *Intermetallics* **2019**, *114*, 106602. [CrossRef]
12. Planes, A.; Mañosa, L.; Moya, X.; Krenke, T.; Acet, M.; Wassermann, E.F. Magnetocaloric effect in Heusler shape-memory alloys. *J. Magn. Magn. Mater.* **2007**, *310*, 2767–2769. [CrossRef]
13. Neves-Bez, H.; Pathak, A.K.; Biswas, A.; Zarkevich, N.; Balema, V.; Mudryk, Y.; Johnson, D.D.; Pecharsky, V.K. Giant enhancement of the magnetocaloric response in Ni–Co–Mn–Ti by rapid solidification. *Acta Mater.* **2019**, *173*, 225–230. [CrossRef]
14. Kaeswurm, B.; Franco, V.; Skokov, K.P.; Gutfleisch, O. Assessment of the magnetocaloric effect in La,Pr(Fe,Si) under cycling. *J. Magn. Magn. Mater.* **2016**, *406*, 259–265. [CrossRef]
15. Gutfleisch, O.; Gottschall, T.; Fries, M.; Benke, D.; Radulov, I.; Skokov, K.P.; Wende, H.; Gruner, M.; Acet, M.; Entel, P.; et al. Mastering hysteresis in magnetocaloric materials. *Philos. Trans. R. Soc. A Math. Phys. Eng. Sci.* **2016**, *374*, 20150308. [CrossRef] [PubMed]
16. Mayergoyz, I. Mathematical models of hysteresis. *IEEE Trans. Magn.* **1986**, *22*, 603–608. [CrossRef]
17. Pike, C.R.; Roberts, A.P.; Verosub, K.L. Characterizing interactions in fine magnetic particle systems using first order reversal curves. *J. Appl. Phys.* **1999**, *85*, 6660–6667. [CrossRef]
18. Dobrotă, C.-I.; Stancu, A. What does a first-order reversal curve diagram really mean? A study case: Array of ferromagnetic nanowires. *J. Appl. Phys.* **2013**, *113*, 43928. [CrossRef]
19. Franco, V.; Gottschall, T.; Skokov, K.P.; Gutfleisch, O. First-Order Reversal Curve (FORC) Analysis of Magnetocaloric Heusler-Type Alloys. *IEEE Magn. Lett.* **2016**, *7*, 1–4. [CrossRef]
20. Franco, V. Temperature-FORC analysis of a magnetocaloric Heusler alloy using a unified driving force approach (T*FORC). *J. Appl. Phys.* **2020**, *127*, 133902. [CrossRef]
21. Atitoaie, A.; Tanasa, R.; Stancu, A.; Enachescu, C. Study of spin crossover nanoparticles thermal hysteresis using FORC diagrams on an Ising-like model. *J. Magn. Magn. Mater.* **2014**, *368*, 12–18. [CrossRef]
22. Preisach, F. Über die magnetische Nachwirkung. *Z. Für Phys.* **1935**, *94*, 277–302. [CrossRef]
23. Pike, C.R.; Roberts, A.P.; Dekkers, M.J.; Verosub, K.L. An investigation of multi-domain hysteresis mechanisms using FORC diagrams. *Phys. Earth Planet. Inter.* **2001**, *126*, 11–25. [CrossRef]
24. Roberts, A.P.; Verosub, K.L. First-order reversal curve diagrams and thermal relaxation effects in magnetic particles. *Geophys. J. Int.* **2001**, *145*, 721–730.

25. Stancu, A.; Pike, C.; Stoleriu, L.; Postolache, P.; Cimpoesu, D. Micromagnetic and Preisach analysis of the First Order Reversal Curves (FORC) diagram. *J. Appl. Phys.* **2003**, *93*, 6620–6622. [CrossRef]
26. Muxworthy, A.; Heslop, D.; Williams, W. Influence of magnetostatic interactions on first-order-reversal-curve (FORC) diagrams: A micromagnetic approach. *Geophys. J. Int.* **2004**, *158*, 888–897. [CrossRef]
27. Newell, A.J. A high-precision model of first-order reversal curve (FORC) functions for single-domain ferromagnets with uniaxial anisotropy. *Geochem. Geophys. Geosyst.* **2005**, *6*, Q05010. [CrossRef]
28. Bean, C.P.; Rodbell, D.S. Magnetic Disorder as a First-Order Phase Transformation. *Phys. Rev.* **1962**, *126*, 104–115. [CrossRef]
29. Piazzi, M.; Bennati, C.; Curcio, C.; Kuepferling, M.; Basso, V. Modeling specific heat and entropy change in La(Fe–Mn–Si)$_{13}$–H compounds. *J. Magn. Magn. Mater.* **2016**, *400*, 349–355. [CrossRef]
30. Karpenkov, D.Y.; Karpenkov, A.Y.; Skokov, K.P.; Radulov, I.A.; Zheleznyi, M.; Faske, T.; Gutfleisch, O. Pressure Dependence of Magnetic Properties in La(Fe,Si)$_{13}$: Multistimulus Responsiveness of Caloric Effects by Modeling and Experiment. *Phys. Rev. Appl.* **2020**, *13*, 34014. [CrossRef]
31. Von Ranke, P.J.; de Campos, A.; Caron, L.; Coelho, A.A.; Gama, S.; de Oliveira, N.A. Calculation of the giant magnetocaloric effect in the MnFeP$_{0.45}$As$_{0.55}$ compound. *Phys. Rev. B* **2004**, *70*, 94410. [CrossRef]
32. Wang, G.F.; Song, L.; Ou, Z.Q.; Zhao, Z.R.; Tegus, O. Calculation of the magnetization and magnetocaloric effect in the MnFeP$_{0.45}$As$_{0.55}$ compound. *Acta Metall. Sin. (Engl. Lett.)* **2007**, *20*, 265–269. [CrossRef]
33. Azzalini, A. *The Skew-Normal and Related Families*; Cambridge University Press: Cambridge, UK, 2013; ISBN 9781107029279.
34. Moreno-Ramírez, L.M.; Blázquez, J.S.; Radulov, I.A.; Skokov, K.P.; Gutfleisch, O.; Franco, V.; Conde, A. Combined Kinetic and Bean-Rodbell approach for describing field-induced transitions in LaFe$_{11.6}$Si$_{1.4}$ alloys. *Submitt. Scr. Mater.* **2020**. submitted for publication.
35. Waske, A.; Giebeler, L.; Weise, B.; Funk, A.; Hinterstein, M.; Herklotz, M.; Skokov, K.; Fähler, S.; Gutfleisch, O.; Eckert, J. Asymmetric first-order transition and interlocked particle state in magnetocaloric La(Fe,Si)$_{13}$. *Phys. Status Solidi Rapid Res. Lett.* **2015**, *9*, 136–140. [CrossRef]
36. Diestel, A.; Niemann, R.; Schleicher, B.; Schwabe, S.; Schultz, L.; Fähler, S. Field-temperature phase diagrams of freestanding and substrate-constrained epitaxial Ni-Mn-Ga-Co films for magnetocaloric applications. *J. Appl. Phys.* **2015**, *118*, 23908. [CrossRef]